Local Atomic Environment of Yb^{3+} in Alkaline-Earth Fluorohalide Nanocrystals

ARTICLE

Local Atomic Environment of Yb³⁺ in Alkaline-Earth Fluorohalide Nanocrystals

Dinesh K. Amarasinghe,[a] K. Tauni Dissanayake,[a] B. Dulani Dhanapala,[a] and Federico A. Rabuffetti[a,†]

The local atomic environment of Yb³⁺ ions doped into Yb:Er:SrFCl, Yb:Er:SrFBr, and Yb:Er:BaFCl nanocrystals was probed using Yb $L2$ edge EXAFS spectroscopy. A structural model derived from substitution of Yb³⁺ for Sr²⁺ or Ba²⁺ in the fluorohalide lattice failed to provide a crystallochemically meaningful description of the first coordination shell of Yb³⁺. On this basis, the presence of Yb³⁺ coordinated as YbF₄Cl₅ or YbF₄Br₅ capped square antiprisms of C_{4v} symmetry was ruled out. Two alternative models were evaluated. The first model was inspired by YbF₉ capped square antiprisms that make up the crystal structure of orthorhombic YbF₃. The second model was based on YbO₄F₃ capped trigonal prisms encountered in monoclinic YbOF. Both models correctly reproduced radial structure functions and yielded chemically meaningful ytterbium–fluorine and ytterbium–oxygen distances. Results from EXAFS studies indicate that compositional and structural heterogeneities appear in the fluorohalide lattice upon aliovalent doping with Yb³⁺. From a compositional standpoint, extra fluoride anions and/or oxide anions appear to be incorporated in the vicinity of Yb³⁺ dopants. From a structural standpoint, the local symmetry around Yb³⁺ (C_s or C_1) is lower than that of the crystallographic sites occupied by alkaline-earth cations. These conclusions hold for three different fluorohalide host compositions and rare-earth doping levels spanning one order of magnitude.

Introduction

Alkaline-earth fluorohalides of formula MFX (M = Ca, Sr, Ba; X = Cl, Br, I) have been extensively used as hosts for divalent rare-earth ions such as Sm²⁺ and Eu²⁺. In fact, chemical substitutions of Sm²⁺ for Ba²⁺ in (Sr,Ba)FCl and of Eu²⁺ for Ba²⁺ in BaFBr have been exploited to realize luminescent pressure sensors[1-4] and X-ray storage phosphors,[5-7] respectively. Fluorohalides doped with trivalent rare-earth ions (RE³⁺) remain comparatively unexplored. Over the past two decades, however, efforts have been undertaken to assess their potential as X-ray storage phosphors,[8-11] optical markers in bioimaging,[12] luminescent thermometers,[13-15] and media for optical data storage.[16-19] Almost invariably, these efforts have focused on nanocrystalline fluorohalides. As a result, advances have been made in the synthesis of RE³⁺-doped alkaline-earth fluorohalide nanocrystals and in the understanding of their photoluminescence and photochemistry. By contrast, structural studies aimed at establishing the placement of RE³⁺ dopants in the fluorohalide lattice lag behind. This information is relevant to delineate metal–metal energy transfer pathways that directly impact photoluminescence response and to establish the structural basis of photochemical reactions, in particular of interactions between RE³⁺ ions and charge-compensating defects that are created with a spatial correlation to the dopant. Early structural studies were conducted on Gd³⁺-doped SrFCl and BaFCl single crystals using electron paramagnetic resonance as a structural probe.[20-23] More recently, fluorescence spectroscopy was employed to gain insight into the local atomic environment of Eu³⁺, Sm³⁺, and Tm³⁺ doped into BaFCl nanocrystals.[8, 9, 18, 24] Although these studies were informative regarding the local symmetry of the site(s) occupied by RE³⁺ ions, they provided limited insight into the chemical identity and spatial distribution of neighboring atoms in the first few coordination shells. Extended X-ray absorption fine structure spectroscopy (EXAFS) is an element-specific technique with the potential to quantitatively probe these structural features. However, to the best of our knowledge, no attempts have been made at using EXAFS to elucidate the local atomic environment of RE³⁺ ions in alkaline-earth fluorohalides.

[a.] Department of Chemistry, Wayne State University, Detroit, MI 48202, USA
† Corresponding author. Email: far@chem.wayne.edu

In this article we report an EXAFS study of the local environment of Yb^{3+} in fluorohalide nanocrystals that had been synthesized by our group and characterized as NIR-to-visible upconverters.[25, 26] Yb *L*2 EXAFS spectra of SrFCl, SrFBr, and BaFCl nanocrystals codoped with Yb^{3+} (sensitizer) and Er^{3+} (activator) are quantitatively modeled. Monometallic clusters derived from the crystal structures of MFX, YbF_3, and YbOF are used to this end. Fits of YbF_4X_5, YbF_9, and YbO_4F_3 clusters to the experimental radial structure functions are carried out and bond distances are extracted. The proposed structural models are compared with respect to their ability to correctly reproduce radial structure functions and to yield a crystallochemically meaningful picture of the first coordination shell of Yb^{3+}. Results from EXAFS studies are discussed from the standpoint of their implication for the placement of Yb^{3+} dopants in the fluorohalide lattice.

Experimental

Nanocrystal Synthesis. Nanocrystals were synthesized following two-step (Yb:Er:SrFCl and Yb:Er:SrFBr) and hot-injection (Yb:Er:BaFCl) routes described in detail elsewhere.[25, 26] Yb:Er:SrFX and Yb:Er:BaFCl nanocrystals that are the focus of this article were synthesized at 250 and 275 °C, respectively. Total rare-earth concentrations and ytterbium-to-erbium ratios determined by inductively coupled plasma mass spectrometry equal 3.7 mol. % and 8.5 (Yb:Er:SrFCl), 0.36 mol. % and 3.5 (Yb:Er:SrFBr), and 3.0 mol. % and 7.0 (Yb:Er:BaFCl), respectively.[25, 26]

Powder X-ray Diffraction (PXRD). PXRD patterns of polycrystalline Yb:Er:SrFX and Yb:Er:BaFCl were collected using a Bruker D2 Phaser diffractometer operated at 30 kV and 10 mA. Cu $K\alpha$ radiation (λ = 1.5418 Å) was employed. A nickel filter was used to remove Cu Kβ. Patterns were collected in the 10−60° 2θ range using a step size of 0.025° and a step time of 0.5 s.

Transmission Electron Microscopy (TEM). TEM images were obtained using a JEOL JEM2010F (JEOL Ltd.) operating at 200 kV. Small aliquots of the native solutions containing the nanocrystals were diluted with toluene and drop-casted onto 200 mesh Cu grids coated with a Lacey carbon film (Ted Pella Inc.).

Extended X-ray Absorption Fine Structure Spectroscopy (EXAFS). EXAFS spectra were collected at the 20−BM−B line of the Advanced Photon Source at Argonne National Laboratory. A Si(111) double crystal monochromator coupled to a harmonic rejection mirror delivered a monochromatic X-ray beam. The beam intensity was detuned to further reduce any residual harmonics. X-ray absorption spectra of fluorohalide nanocrystals were collected in fluorescence mode at the Yb *L*2 edge (9978 eV). Bulk YbF_3 (99.9%, Sigma Aldrich) was measured in transmission mode as a reference. Spectra were recorded between 9828 and 10435 eV. Normalized EXAFS spectra $\chi(k)$ were extracted from the raw data using Athena.[27] EXAFS analyses were performed on radial structure functions (RSFs) $\chi(r)$ obtained after computing the Fourier transforms of k^2- and k^3-weighted $\chi(k)$. Fourier transforms were computed in
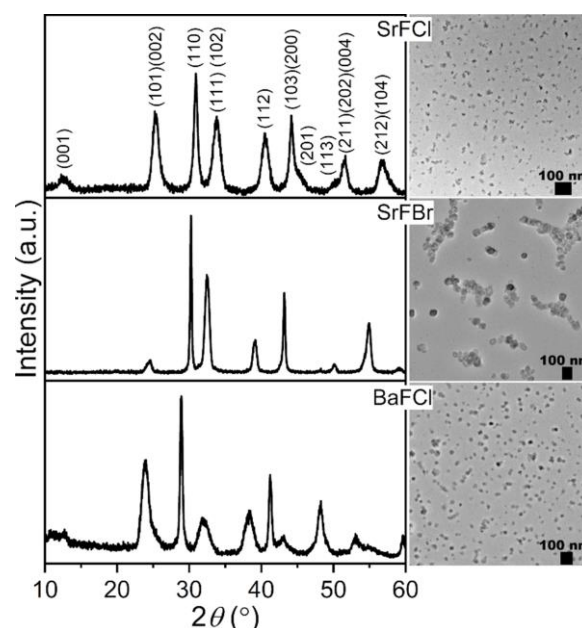

Figure 1. Indexed PXRD patterns and TEM images of SrFCl, SrFBr, and BaFCl nanocrystals codoped with Yb^{3+} and Er^{3+}.

the 2.0–9.5 Å^{-1} k range. A Hanning window with dk = 0.1 Å^{-1} was used. Single-shell, single-scattering models were employed to fit $\chi(r)$ functions using Artemis.[27] Structural models included YbF_4X_5, YbF_9, and YbO_4F_3 monometallic clusters derived from the corresponding MFX, YbF_3, and YbOF structures. These models were fit to $\chi(r)$ by refining (1) the amplitude reduction factor S_0^2, (2) the threshold energy shift ΔE_0, (3) fractional atomic coordinates, and (4) Debye–Waller factors (σ^2). The number of backscatterer atoms in each model was fixed at the value obtained from the corresponding crystal structure. Crystal structures and clusters were visualized using VESTA.[28]

Results and Discussion

Detailed quantitative analyses of the long- and short-range crystal structures, elemental compositions, and morphologies of Yb:Er:SrFX and Yb:Er:BaFCl nanocrystals were reported by us in previous articles.[25, 26] Herein, we only provide a brief summary of X-ray diffraction and electron microscopy analyses aimed at screening phase purity and morphology. Results from these analyses are summarized in **Figure 1**. All three samples appear single phase to PXRD. All diffraction maxima can be indexed to the corresponding SrFCl (PDF No. 00–024–1192), SrFBr (PDF No. 01–076–1287), and BaFCl (PDF No. 00–024–0096) tetragonal phases. TEM imaging shows that fluorochloride nanocrystals are significantly smaller than their fluorobromide counterpart. Average sizes equal to 15.8 ± 4.20 (SrFCl), 55.3 ± 12.4 (SrFBr), and 19.5 ± 3.70 nm (BaFCl) were determined through analysis of ≈300 nanocrystals in each sample.[25, 26]

Different local atomic environments were envisioned for Yb^{3+} doped into SrFCl, SrFBr, and BaFCl nanocrystals. To begin with, we assumed substitution of Yb^{3+} for Sr^{2+} or Ba^{2+} and a first coordination shell of stoichiometry YbF_4X_5. This model is
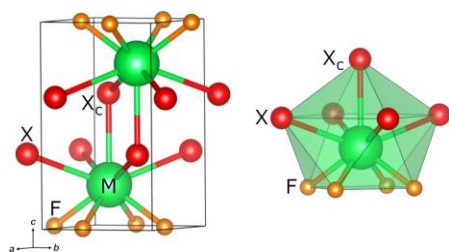
Figure 2. Unit cell of MFX (left) and view of the first coordination shell of M^{2+} as an MF_4X_5 polyhedron (right).

Table 1. Atomic Coordinates in MFX[a]

Atom	x	y	z	Site Symmetry
M	1/4	1/4	≈0.20	$4mm$
F	3/4	1/4	0	$\bar{4}m2$
X	1/4	1/4	≈0.64	$4mm$

[a]Lattice constants: a = 4.1259 Å and c = 6.9579 Å (SrFCl), a = 4.2610 Å and c = 7.4820 Å (SrFBr), and a = 4.3847 Å and c = 7.2488 Å (BaFCl).
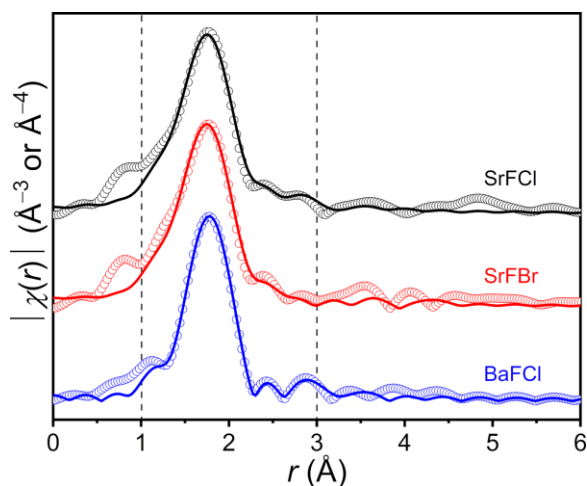

Figure 3. Fits of an YbF_4X_5 monometallic cluster to the radial structure functions of Yb:Er:SrFX and Yb:Er:BaFCl nanocrystals. Experimental (hollow circles) and calculated functions (solid lines) are shown. $\chi(r)$ functions were fit in the 1.0–3.0 Å r range (depicted with vertical dashed lines).

directly derived from the crystal structure of alkaline-earth fluorohalides as shown in **Figure 2**. Atomic coordinates of crystallographically distinct atoms in this structure are given in **Table 1**. MFX features a tetragonal unit cell elongated along the c axis (space group $P4/nmm$). The building block of the structure consists of MF_4X_5 capped square antiprisms of C_{4v} symmetry. The first coordination shell of the alkaline-earth metal includes four fluoride (F) and five heavy halide anions

Table 2. Structural Parameters of YbF_4X_5 Monometallic Clusters

	SrFCl	SrFBr	BaFCl
S_0^2	1.59(18)	1.44(15)	1.77(12)
ΔE_0 (eV)	−1.2(1.0)	−1.0(1.0)	−0.9(7)
zYb	0.119(5)	0.081(6)	0.048(5)
zX	0.587(10)	0.50(2)	0.709(19)
σ^2_F (Å^2)	0.013(2)	0.012(2)	0.0095(10)
σ^2_X (Å^2)	0.03(2)	0.03(3)	0.037(12)
Yb–F (Å) (×4)	2.223(14)	2.215(13)	2.220(7)
Yb–X (Å) (×4)	3.56(5)	4.37(13)	3.57(7)
Yb–X_c (Å) (×1)	3.26(8)	3.10(18)	4.79(15)
Bond valence sum[a]	1.81	1.79	1.73
Fit residual R (%)	0.9	0.8	0.4

[a] Bond valence parameters: R_o = 1.875 Å (Yb–F), 2.371 Å (Yb–Cl), 2.451 Å (Yb–Br), and b = 0.37 Å.

(X). One of the heavy halides (X_c) sits directly above the metal cation. The presence of two anionic ligands of significantly different radii ($r(F^-)$ = 1.31 Å, $r(Cl^-)$ = 1.81 Å, and $r(Br^-)$ = 1.96 Å)[29] leads to a bimodal distribution of metal–halogen bond distances. As an example, SrFCl features Sr–F and Sr–Cl distances equal to ≈2.51 and 3.10 Å, respectively.[25] This distribution of bond distances is clearly observed as the first two maxima in the radial structure functions of Yb:Er:SrFX and Yb:Er:BaFCl nanocrystals extracted from EXAFS spectra collected at the Sr K and Ba $L3$ edges, respectively.[25, 26] By contrast, a single maximum is observed in the RSFs derived from EXAFS spectra recorded at the Yb $L2$ edge, as shown in **Figure 3**. This maximum results from an isotropic distribution of ytterbium–ligand distances which, in turn, reflects the presence of nearest neighbors of identical or similar ionic radii around ytterbium. On this basis, incorporation of Yb^{3+} into alkaline-earth fluorohalide nanocrystals as YbF_4X_5 may be ruled out. Notwithstanding, results from fits of this model to the experimental RSFs of Yb:Er:SrFX and Yb:Er:BaFCl nanocrystals are provided for completeness. $\chi(r)$ functions were fit in the 1.0–3.0 Å r range. Atomic coordinates zYb and zX were refined. Fits are shown in **Figure 3** and the resulting structural parameters are provided in **Table 2**; the corresponding k^2- and k^3-weighted $\chi(k)$ functions are given in the ESI (**Figure S1**). Although inspection of fits indicates an adequate agreement between experimental and calculated RSFs, the resulting Yb–Cl and Yb–Br distances are abnormally long. Further, these distances are longer than Sr–Cl (≈3.10 Å) and Sr–Br distances (≈3.22–3.46 Å) encountered in SrFCl and SrFBr nanocrystals, respectively, despite the fact that the ionic radius of Yb^{3+} (1.04 Å) is smaller than that of Sr^{2+} (1.31 Å).[29] Likewise, Yb–Cl distances are longer than Ba–Cl distances in BaFCl nanocrystals (≈3.20–3.5 Å) even though Ba^{2+} (1.47 Å) is significantly larger than Yb^{3+}.[26] As expected, bond valence sums computed using ytterbium–ligand distances extracted from EXAFS analyses yield an anomalous underbonding of Yb^{3+}, with values ranging between 1.73 and 1.81 v.u. Altogether, these results demonstrate that the first coordination shell of Yb^{3+} in Yb:Er:SrFX and Yb:Er:BaFCl nanocrystals cannot be described using an YbF_4X_5 cluster.

Emphasis was then placed on finding crystallochemically meaningful structural models. Based on the observation of a single maximum in the experimental RSFs of Yb:Er:SrFX and Yb:Er:BaFCl nanocrystals, we sought for structures in which Yb^{3+} features a single ligand type in its first coordination shell or, alternatively, two different ligands with similar ionic radii. With this consideration in mind, we selected YbF_3 (PDF No. 00–034–0102) as our first alternative. Its crystal structure is shown in **Figure 4**. Atomic coordinates of crystallographically distinct atoms are given in **Table 3**. YbF_3 presents an orthorhombic unit cell (space group $Pnma$). The building block of the structure consists of YbF_9 distorted capped square antiprisms of C_s symmetry. This polyhedron features six distinct Yb–F bond distances, five of which range between 2.22 and 2.29 Å; the remaining distance equals 2.61 Å. The feasibility of employing an YbF_9 cluster to describe the first coordination shell of Yb^{3+} in Yb:Er:SrFX and Yb:Er:BaFCl nanocrystals was quantitatively
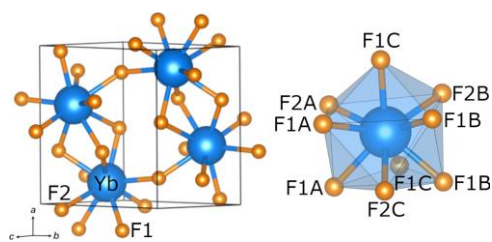
Figure 4. Unit cell of YbF$_3$ (left) and view of the first coordination shell of Yb^{3+} as an YbF$_9$ polyhedron (right).

Table 3. Atomic Coordinates in YbF$_3$[a]

Atom	x	y	z	Site Symmetry
Yb	0.36724	1/4	0.05376	.m.
F1	0.1646	0.0633	0.3675	1
F2	0.0269	1/4	0.901	.m.

[a] Lattice constants: a = 6.218 Å, b = 6.785 Å, and c = 4.431 Å.

assessed. A monometallic cluster YbF$_9$ was fit to the experimental RSFs of these nanocrystals. Bulk YbF$_3$ was also analyzed for comparison purposes. Fits were carried out in the 1.0–2.7 Å r range and atomic coordinates xYb and zYb were refined. Fits are shown in **Figure 5** and the resulting structural parameters are provided in **Table 4**. Fits of YbF$_3$ and k^3-weighted $\chi(k)$ functions are given in the ESI (**Figures S2 and S3**). Inspection of the fits and values of the refined structural parameters point to YbF$_9$ as a plausible model for the local coordination of Yb^{3+}. Yb–F bond distances extracted for Yb:Er:SrFX and Yb:Er:BaFCl nanocrystals are in the 2.15–2.58 Å range, in line with those derived for bulk YbF$_3$ (2.18–2.61 Å). Further, bond valence analyses yield valence sums of 2.95 (SrFCl), 2.95 (SrFBr), and 3.00 v.u. (BaFCl) in excellent agreement with the expected value of 3.00. YbF$_9$ therefore appears as a meaningful description of the first coordination shell of Yb^{3+} doped into alkaline-earth fluorohalide nanocrystals that are the focus of this investigation.

The second alternative model we considered is based on YbOF (PDF No. 01–082–1465). Its crystal structure is shown in

Table 4. Structural Parameters of YbF$_9$ Monometallic Clusters

	SrFCl	SrFBr	BaFCl	YbF$_3$
S_0^2	1.25(12)	1.14(17)	1.3(2)	1.20(8)
ΔE_0 (eV)	2.9(1.0)	3.8(8)	3.5(1.0)	2.8(7)
xYb	0.361(3)	0.384(5)	0.390(3)	0.358(8)
zYb	0.066(7)	0.054(13)	0.051(7)	0.060(12)
σ^2_F (Å^2)	0.010(3)	0.008(5)	0.001(5)	0.008(5)
Yb–F1A (Å) (×2)	2.21(3)	2.32(4)	2.35(3)	2.22(5)
Yb–F1B (Å) (×2)	2.293(18)	2.19(3)	2.155(17)	2.31(5)
Yb–F1C (Å) (×2)	2.307(13)	2.30(3)	2.301(12)	2.30(3)
Yb–F2A (Å) (×1)	2.20(3)	2.32(4)	2.35(3)	2.18(5)
Yb–F2B (Å) (×1)	2.31(4)	2.20(6)	2.17(3)	2.30(6)
Yb–F2C (Å) (×1)	2.58(4)	2.58(6)	2.57(3)	2.61(6)
Bond valence sum[a]	2.95	2.95	3.00	2.93
Fit residual R (%)	0.5	1.1	0.7	0.2

[a] Bond valence parameters: R_o = 1.875 Å (Yb–F) and b = 0.37 Å.

Figure 6 and atomic coordinates of crystallographically distinct atoms are given in **Table 5**. YbOF features a monoclinic unit cell (space group $P2_1/c$) and YbO$_4$F$_3$ distorted capped trigonal prisms of C_1 symmetry as the building block. In bulk, Yb–O and Yb–F bond distances span narrow ranges between 2.19 and 2.26 Å and between 2.25 and 2.37 Å, respectively. On this basis, an YbO$_4$F$_3$ cluster appeared as a plausible alternative to
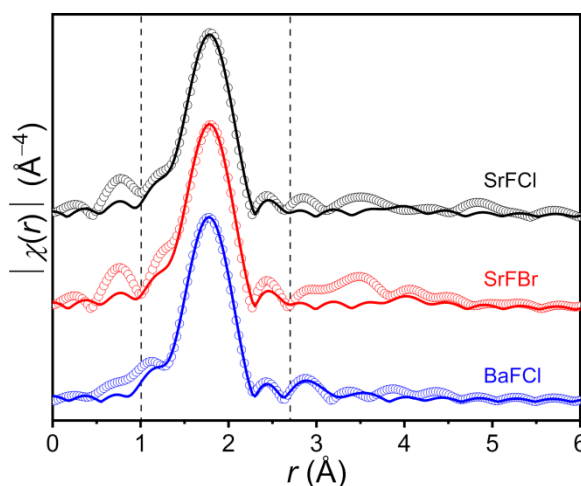

Figure 5. Fits of an YbF$_9$ cluster to the radial structure functions of Yb:Er:SrFX and Yb:Er:BaFCl nanocrystals. Experimental (hollow circles) and calculated functions (solid lines) are shown. $\chi(r)$ functions were fit in the 1.0–2.7 Å r range (depicted with vertical dashed lines).

fit the single maximum observed in the experimental RSFs of Yb:Er:SrFX and Yb:Er:BaFCl nanocrystals. Moreover, pure and rare-earth-doped single crystal and bulk alkaline-earth fluorohalides have been shown to incorporate oxide anions as an impurity or as a charge-compensating species.[23, 30-34] Oxygen incorporation has been observed even in pristine single crystals grown under conditions significantly more stringent than those employed in the synthesis of our nanocrystals;[35, 36] hence, the presence of oxide anions in the latter cannot be ruled out. In fact, oxide anions substituting for chloride have been suggested as charge-compensating defects in Sm^{3+}-doped BaFCl single crystals and nanocrystals.[8, 18] EXAFS fits of YbO$_4$F$_3$ to the experimental RSFs functions of Yb:Er:SrFX

Figure 6. Unit cell of YbOF (left) and view of the first coordination shell of Yb^{3+} as an YbO$_4$F$_3$ polyhedron (right).
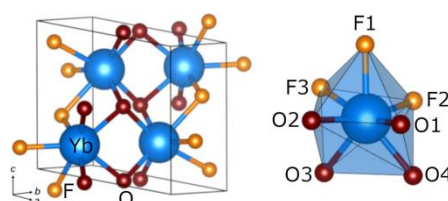
and Yb:Er:BaFCl are shown in **Figure 7**. Refined structural parameters are given in **Table 6**. Fits were carried out in the 1.0–2.7 Å r range and atomic coordinates xYb and zYb were refined. Good agreement is observed between experimental and calculated RSFs. Chemically sensible Yb–O and Yb–F bond distances ranging between 2.16 and 2.40 Å are obtained. Bond valence sums computed using these distances range between 2.86 and 2.92 v.u., close to the expected value of 3.00 for Yb^{3+}. YbO_4F_3 therefore appears as a reasonable candidate to describe the first coordination shell of Yb^{3+} in Yb:Er:SrFX and Yb:Er:BaFCl nanocrystals. Comparison of the structural parameters refined for YbF_9 and YbO_4F_3 clusters shows that bond valence sums computed for the former are systematically closer to 3.00 than those calculated for the latter. In addition, although Debye–Waller factors refined for fluoride and oxide ligands in YbO_4F_3 are positively defined, their uncertainties are large relative to those obtained for
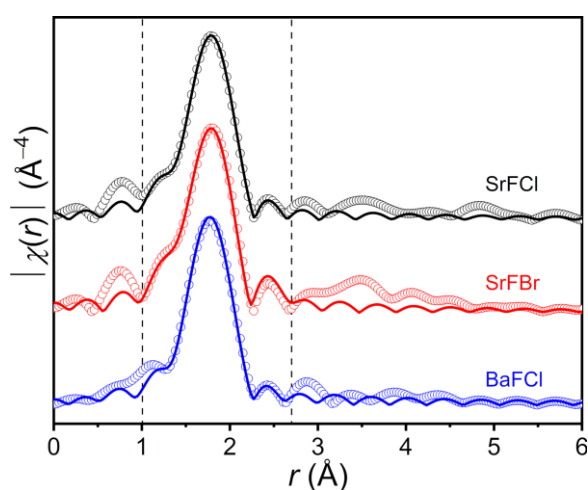
fluoride anions in YbF_9. Fixing the amplitude reduction factor S_0^2 mitigates this deficiency by decreasing the number of refined parameters from 6 to 5, but does not completely eliminate it. Thus, on the basis of EXAFS analyses, one may favor YbF_9 over YbO_4F_3 as the most plausible coordination environment of Yb^{3+} in fluorohalide nanocrystals, even though the latter model cannot be ruled out.

Conclusions

In summary, the local atomic environment of Yb^{3+} ions doped into Yb:Er:SrFX and Yb:Er:BaFCl nanocrystals was investigated using Yb L2 edge EXAFS spectroscopy. An YbF_4X_5 structural model derived from substitution of Yb^{3+} for Sr^{2+} or Ba^{2+} in the MFX lattice failed to correctly reproduce radial structure functions and led to chemically meaningless Yb–X distances. This result provided conclusive evidence of the absence of YbF_4X_5 polyhedra. Two alternative models yielded crystallochemically meaningful descriptions of the first coordination shell of Yb^{3+}. The first model consisted of Yb^{3+} embedded in a fluoride-rich environment and was inspired by YbF_9 polyhedra that make up the crystal structure of YbF_3. The second model was based on YbO_4F_3 polyhedra encountered in crystalline YbOF and had Yb^{3+} sit in an oxygen-rich environment. Both models pointed to the appearance of compositional and structural heterogeneities in the fluorohalide lattice upon aliovalent doping with Yb^{3+}. Compositional heterogeneities involve incorporation of extra fluoride anions and/or of oxide anions to satisfy the electronic requirements of Yb^{3+}, a stronger Lewis acid than Sr^{2+} and Ba^{2+}. Structural heterogeneities are reflected by a reduction of the local symmetry around the trivalent dopant, as the point group of Yb^{3+} (C_s or C_1) is of lower symmetry than that of the crystallographic sites occupied by alkaline-earth cations (C_{4v}). A similar result has been reported for Eu^{3+}:BaFCl nanocrystals.[24] These conclusions hold for alkaline-earth fluorohalide nanocrystals that feature three different hosts (SrFCl, SrFBr, and BaFCl) and rare-earth doping levels spanning one order of magnitude (≈0.36 to 3.7 mol. %).

Questions that remain open include whether Yb^{3+} ions are isolated or aggregated (i.e., what is the connectivity of YbF_9, YbO_4F_3, or YbO_nF_m polyhedra) and their location in the nanocrystals (i.e., inner lattice vs. surface). Regarding the latter, it is worth noting that the absence of strong maxima in the radial structure functions past the first coordination shell suggests a high degree of positional disorder. This is consistent with Yb^{3+} ions sitting on the nanocrystals' surface or in inner lattice sites with a highly distorted atomic environment.

Figure 7. Fits of an YbO_4F_3 cluster to the radial structure functions of Yb:Er:SrFX and Yb:Er:BaFCl nanocrystals. Experimental (hollow circles) and calculated functions (solid lines) are shown. $\chi(r)$ functions were fit in the 1.0–2.7 Å r range (depicted with vertical dashed lines).

Table 6. Structural Parameters of YbO_4F_3 Monometallic Clusters

	SrFCl	SrFBr	BaFCl
S_0^2	1.50(10)	1.4(3)	2.1(5)
ΔE_0 (eV)	1.8(6)	2.0(1.1)	1.6(1.2)
xYb	0.282(6)	0.305(2)	0.293(9)
zYb	0.235(4)	0.217(6)	0.234(12)
σ^2_F (Å^2)	0.017(7)	0.001(7)	0.05(7)
σ^2_O (Å^2)	0.0056(15)	0.004(0.010)	0.005(5)
Yb–F1 (Å) (×1)	2.16(3)	2.253(15)	2.20(5)
Yb–F2 (Å) (×1)	2.20(3)	2.33(2)	2.24(5)
Yb–F3 (Å) (×1)	2.40(3)	2.38(3)	2.42(6)
Yb–O1 (Å) (×1)	2.16(3)	2.18(3)	2.14(5)
Yb–O2 (Å) (×1)	2.33(3)	2.21(3)	2.30(6)
Yb–O3 (Å) (×1)	2.40(4)	2.25(3)	2.35(6)
Yb–O4 (Å) (×1)	2.25(3)	2.24(3)	2.22(5)
Bond valence sum^a	2.86	2.92	2.90
Fit residual R (%)	0.2	0.6	0.4

^{a} Bond valence parameters: R_o = 1.875 Å (Yb–F), 1.965 Å (Yb–O), and b = 0.37 Å.

Conflicts of interest

There are no conflicts to declare.

Acknowledgements

ARTICLE

Notes and references

1 Shen, Y. R.; Gregorian, T.; Holzapfel, W. B. In *Progress in Pressure Measurements with Luminescence Sensors*, 28th Annual Meeting of the European High Pressure Research Group – 1st European Technology Forum: High Pressure and Materials, Bordeaux, France, 1990; Bordeaux, France, 1990; p 73−75.
2 Shen, Y. R.; Holzapfel, W. B., Effect of Pressure on the $^{7}F_{1}$ Multiplet and Phonon Sidebands of Sm^{2+} in BaFCl. *Journal of Alloys and Compounds* **1993,** 192, (1), 53−54.
3 Comodi, P.; Zanazzi, P. F., Improved Calibration Curve for the Sm^{2+}-BaFCl Pressure Sensor. *Journal of Applied Crystallography* **1993,** 26, 843−845.
4 Lorenz, B.; Shen, Y. R.; Holzapfel, W. B., Characterization of the New Luminescence Pressure Sensor $SrFCl:Sm^{2+}$. *High Pressure Research* **1994,** 12, (2), 91−99.
5 Sonoda, M.; Takano, M.; Miyahara, J.; Kato, H., Computed Radiography Utilizing Scanning Laser Stimulated Luminescence. *Radiology* **1983,** 148, (3), 833−838.
6 Takahashi, K.; Kohda, K.; Miyahara, J.; Kanemitsu, Y.; Amitani, K.; Shionoya, S., Mechanism of Photostimulated Luminescence in $BaFX:Eu^{2+}$ (X = Cl, Br) Phosphors. *Journal of Luminescence* **1984,** 31−32, 266−268.
7 Takahashi, K.; Miyahara, J.; Shibahara, Y., Photostimulated Luminescence (PSL) and Color Centers in $BaFX:Eu^{2+}$ (X = Cl, Br, I) Phosphors. *Journal of the Electrochemical Society* **1985,** 132, (6), 1492−1494.
8 Liu, Z.; Stevens-Kalceff, M. A.; Riesen, H., Effects of Postannealing on the Photoluminescence Properties of Coprecipitated Nanocrystalline $BaFCl:Sm^{3+}$. *The Journal of Physical Chemistry A* **2013,** 117, (9), 1930−1934.
9 Zhang, J.; Riesen, H., Controlled Generation of Tm^{2+} Ions in Nanocrystalline $BaFCl:Tm^{3+}$ by X-ray Irradiation. *The Journal of Physical Chemistry A* **2017,** 121, 803−809.
10 Zhang, J.; Riesen, N.; Riesen, H., Mechanochemically Prepared SrFCl Nanophosphor Co-Doped with Yb^{3+} and Er^{3+} for Detecting Ionizing Radiation by Upconversion Luminescence. *Nanoscale* **2017,** 9, (41), 15958−15966.
11 Riesen, H.; Kaczmarek, W. A., Efficient X-ray Generation of Sm^{2+} in Nanocrystalline $BaFCl/Sm^{3+}$: A Photoluminescent X-ray Storage Phosphor. *Inorganic Chemistry* **2007,** 46, (18), 7235−7237.
12 Zhao, X.; Yu, Q.; Yuan, J.; Thakor, N. V.; Tan, M. C., Biodegradable Rare Earth Fluorochloride Nanocrystals for Phototheranostics. *RSC Advances* **2020,** 10, (26), 15387−15393.
13 Perera, S. S.; Dissanayake, K. T.; Rabuffetti, F. A., Alkaline-Earth Fluorohalide Nanocrystals for Upconversion Thermometry. *Journal of Luminescence* **2019,** 207, 416−423.
14 Dhanapala, B. D.; Munasinghe, H. N.; Dissanayake, K. T.; Suescun, L.; Rabuffetti, F. A., Expanding the Synthetic Toolbox to Access Pristine and Rare-Earth-Doped BaFBr

Nanocrystals. *Dalton Transactions* **2021,** 50, (44), 16092−16098.
15 Dhanapala, B. D.; Munasinghe, H. N.; Rabuffetti, F. A., Temperature-Dependent Luminescence of CaFCl:Yb,Er Upconverting Nanocrystals. *Journal of Luminescence* **2021,** 235, 117974.
16 Wang, X.; Riesen, H.; Stevens-Kalceff, M. A.; Rajan, R. P., Room Temperature Hole-Burning of X-ray Induced Sm^{2+} in Nanocrystalline $Ba_{0.5}Sr_{0.5}FCl_{0.5}Br_{0.5}:Sm^{3+}$ Prepared by Mechanochemistry. *The Journal of Physical Chemistry A* **2014,** 118, (40), 9445−9450.
17 Riesen, N.; François, A.; Badek, K.; Monro, T. M.; Riesen, H., Photoreduction of Sm^{3+} in Nanocrystalline BaFCl. *The Journal of Physical Chemistry A* **2015,** 119, (24), 6252−6256.
18 Riesen, H.; Badek, K.; Monro, T. M.; Riesen, N., Highly Efficient Valence State Switching of Samarium in BaFCl:Sm Nanocrystals in the Deep UV for Multilevel Optical Data Storage. *Optical Materials Express* **2016,** 6, (10), 3097−3108.
19 Riesen, N.; Badek, K.; Riesen, H., Data Storage in a Nanocrystalline Mixture Using Room Temperature Frequency-Selective and Multilevel Spectral Hole-Burning. *ACS Photonics* **2021,** 8, (10), 3078−3084.
20 Nicollin, D.; Bill, H., Gd^{3+}, Eu^{2+} in SrFCl and BaFCl Single Crystals: EPR Results. *Solid State Communications* **1976,** 20, (2), 135−137.
21 Zevenhuijzen, D.; Vanwinsum, J. A.; Hartog, H. W. D., S-State Ions in Tetragonal SrFCl. *Journal of Physics C: Solid State Physics* **1976,** 9, (16), 3113−3119.
22 Nicollin, D.; Bill, H., Experimental Contribution to the Study of the S-State Ions in Ionic Single Crystals. *Journal of Physics C: Solid State Physics* **1978,** 11, (23), 4803−4814.
23 Falin, M.; Bill, H.; Lovy, D., EPR of Sm^{3+} in BaFCl Single Crystals. *Journal of Physics: Condensed Matter* **2004,** 16, (8), 1293−1298.
24 Ju, Q.; Liu, Y. S.; Li, R. F.; Liu, L. Q.; Luo, W. Q.; Chen, X. Y., Optical Spectroscopy of Eu^{3+}-Doped BaFCl Nanocrystals. *The Journal of Physical Chemistry C* **2009,** 113, (6), 2309−2315.
25 Dissanayake, K. T.; Rabuffetti, F. A., Multicolor Emission in Chemically and Structurally Tunable Er:Yb:SrFX (X = Cl, Br) Upconverting Nanocrystals. *Chemistry of Materials* **2018,** 30, (7), 2453−2462.
26 Dissanayake, K. T.; Amarasinghe, D. K.; Suescun, L.; Rabuffetti, F. A., Accessing Mixed-Halide Upconverters Using Heterohaloacetate Precursors. *Chemistry of Materials* **2019,** 31, (16), 6262−6267.
27 Ravel, B.; Newville, M., ATHENA, ARTEMIS, HEPHAESTUS: Data Analysis for X-ray Absorption Spectroscopy Using IFEFFIT. *Journal of Synchrotron Radiation* **2005,** 12, (4), 537−541.
28 Momma, K.; Izumi, F., VESTA 3 for Three-dimensional Visualization of Crystal, Volumetric and Morphology Data. *Journal of Applied Crystallography* **2011,** 44, 1272−1276.
29 Shannon, R. D., Revised Effective Ionic-Radii and Systematic Studies of Interatomic Distances in Halides and Chalcogenides. *Acta Crystallographica Section A* **1976,** 32, 751−767.
30 Catlow, C. R. A., Oxygen Incorporation in the Alkaline-Earth Fluorohalides. *Journal of Physics and Chemistry of Solids* **1977,** 38, (10), 1131−1136.
31 Eachus, R. S.; McDugle, W. G.; Nuttall, R. H. D.; Olm, M. T.; Koschnick, F. K.; Hangleiter, T.; Spaeth, J. M., Radiation-Produced Electron and Hole-Centers in Oxygen-Containing BaFBr. 1. ER and ODEPR Studies. *Journal of Physics: Condensed Matter* **1991,** 3, (47), 9327−9338.
32 Eachus, R. S.; McDugle, W. G.; Nuttall, R. H. D.; Olm, M. T.; Koschnick, F. K.; Hangleiter, T.; Spaeth, J. M., Radiation-Produced Electron and Hole-Centers in Oxygen-Containing

BaFBr. 2. An ENDOR Study of O⁻(F). *Journal of Physics: Condensed Matter* **1991,** 3, (47), 9339–9349.

33 Radzhabov, E.; Otroshok, V., Optical-Spectra of Oxygen Defects in BaFCl and BaFBr Crystals. *Journal of Physics and Chemistry of Solids* **1995,** 56, (1), 1–7.

34 Chen, X. Y.; Zhao, W.; Cook, R. E.; Liu, G. K., Anomalous Luminescence Dynamics of Eu³⁺ in BaFCl Microcrystals. *Physical Review B* **2004,** 70, (20), 205122.

35 Koschnick, F. K.; Hangleiter, T.; Song, K. S.; Spaeth, J., Optically Detected Magnetic Resonance Study of an Oxygen−Vacancy Complex in BaFBr. *Journal of Physics: Condensed Matter* **1995,** 7, (34), 6925–6937.

36 Eachus, R. S.; Nuttall, R. H. D.; Olm, M. T.; McDugle, W. G.; Koschnick, F. K.; Hangleiter, T.; Spaeth, J. M., Oxygen Defects in BaFBr and BaFCl. *Physical Review B* **1995,** 52, (6), 3941–3950.